AD-A038 844 OAKLAND UNIV ROCHESTER MICH SCHOOL OF ENGINEERING F/G 20/11
ON THE INTERPRETATION OF SHADOW-MOIRE FRINGES,(U)
APR 77 J BUITRAGO, A J DURELLI N00014-76-C-0487
UNCLASSIFIED 42 NL

| OF |
AD
A038844

END

DATE
FILMED
5-77

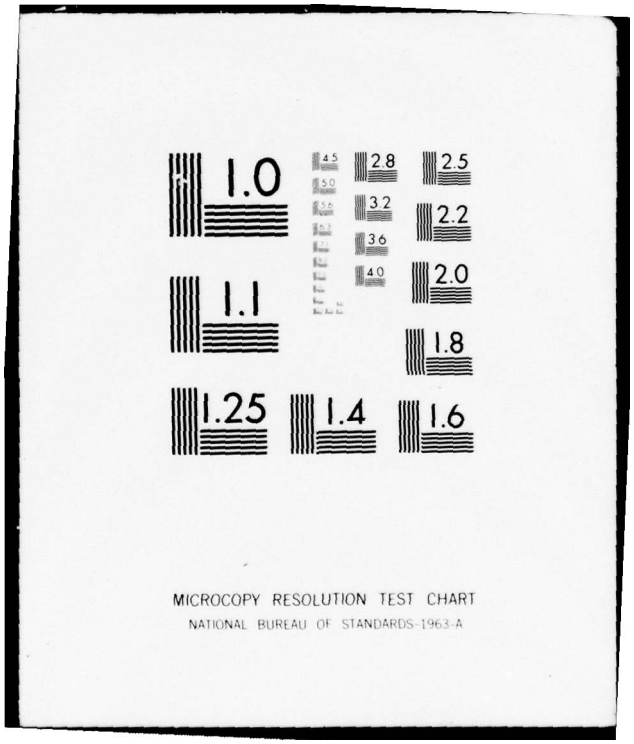
1.0
1.1
1.25
1.4
1.6
1.8
2.0
2.2
2.5
2.8
3.2
3.6
4.0
4.5
5.0
MICROCOPY RESOLUTION TEST CHART
NATIONAL BUREAU OF STANDARDS-1963-A

(3) 9

ON THE INTERPRETATION OF SHADOW-MOIRÉ FRINGES

BY

J. BUITRAGO AND A. J. DURELLI

SPONSORED BY

OFFICE OF NAVAL RESEARCH
DEPARTMENT OF THE NAVY
WASHINGTON, D.C. 20025

ON

CONTRACT No. N00014-76-C-0487
O.U. PROJECT No. 30339-49
REPORT No. 42

SCHOOL OF ENGINEERING
OAKLAND UNIVERSITY
ROCHESTER, MICHIGAN 48063

APRIL 1977

ON THE INTERPRETATION OF SHADOW-MOIRÉ FRINGES

by

J. Buitrago and A. J. Durelli

Sponsored by

Office of Naval Research
Department of the Navy
Washington, D.C. 20025

on

Contract No. N00014-76-C-0487
O.U. Project No. 30339-49
Report No. 42

School of Engineering
Oakland University
Rochester, Michigan 48063

April 1977

ON THE INTERPRETATION OF SHADOW-MOIRÉ FRINGES

by

J. Buitrago and A. J. Durelli

ABSTRACT

Shadow-moiré is presented as one of several means of determining loci of constant height in curved surfaces (isotathmics). A general expression to interpret the fringes is derived taking into consideration possible rotations and translation of the grating. A discussion of the influence of such rotations and translation on the sensitivity of the response is also presented. Furthermore, simplified equations are obtained for particular cases of practical interest. An example of application to the case of an inverted perforated tube is shown.

Previous Technical Reports to the Office of Naval Research

1. A. J. Durelli, "Development of Experimental Stress Analysis Methods to Determine Stresses and Strains in Solid Propellant Grains"--June 1962.
   Developments in the manufacturing of grain-propellant models are reported. Two methods are given: a) cementing routed layers and b) casting.

2. A. J. Durelli and V. J. Parks, "New Method to Determine Restrained Shrinkage Stresses in Propellant Grain Models"--October 1962.
   The birefringence exhibited in the curing process of a partially restrained polyurethane rubber is used to determine the stress associated with restrained shrinkage in models of solid propellant grains partially bonded to the case.

3. A. J. Durelli, "Recent Advances in the Application of Photoelasticity in the Missile Industry"--October 1962.
   Two- and three-dimensional photoelastic analysis of grains loaded by pressure and by temperature are presented. Some applications to the optimization of fillet contours and to the redesign of case joints are also included.

4. A. J. Durelli and V. J. Parks, "Experimental Solution of Some Mixed Boundary Value Problems"--April 1964.
   Means of applying known displacements and known stresses to the boundaries of models used in experimental stress analysis are given. The application of some of these methods to the analysis of stresses in the field of solid propellant grains is illustrated. The presence of the "pinching effect" is discussed.

5. A. J. Durelli, "Brief Review of the State of the Art and Expected Advance in Experimental Stress and Strain Analysis of Solid Propellant Grains"--April 1964.
   A brief review is made of the state of the experimental stress and strain analysis of solid propellant grains. A discussion of the prospects for the next fifteen years is added.

6. A. J. Durelli, "Experimental Strain and Stress Analysis of Solid Propellant Rocket Motors"--March 1965.
   A review is made of the experimental methods used to strain-analyze solid propellant rocket motor shells and grains when subjected to different loading conditions. Methods directed at the determination of strains in actual rockets are included.

7. L. Ferrer, V. J. Parks and A. J. Durelli, "An Experimental Method to Analyze Gravitational Stresses in Two-Dimensional Problems"--October 1965.
   Photoelasticity and moiré methods are used to solve two-dimensional problems in which gravity-stresses are present.

8. A. J. Durelli, V. J. Parks and C. J. del Rio, "Stresses in a Square Slab Bonded on One Face to a Rigid Plate and Shrunk"--November 1965.
A square epoxy slab was bonded to a rigid plate on one of its faces in the process of curing. In the same process the photoelastic effects associated with a state of restrained shrinkage were "frozen-in." Three-dimensional photoelasticity was used in the analysis.

9. A. J. Durelli, V. J. Parks and C. J. del Rio, "Experimental Determination of Stresses and Displacements in Thick-Wall Cylinders of Complicated Shape"--April 1966.
Photoelasticity and moiré are used to analyze a three-dimensional rocket shape with a star shaped core subjected to internal pressure.

10. V. J. Parks, A. J. Durelli and L. Ferrer, "Gravitational Stresses Determined Using Immersion Techniques"--July 1966.
The methods presented in Technical Report No. 7 above are extended to three-dimensions. Immersion is used to increase response.

11. A. J. Durelli and V. J. Parks. "Experimental Stress Analysis of Loaded Boundaries in Two-Dimensional Second Boundary Value Problems"--February 1967.
The pinching effect that occurs in two-dimensional bonding problems, noted in Reports 2 and 4 above, is analyzed in some detail.

12. A. J. Durelli, V. J. Parks, H. C. Feng and F. Chiang, "Strains and Stresses in Matrices with Inserts,"-- May 1967.
Stresses and strains along the interfaces, and near the fiber ends, for different fiber end configurations, are studied in detail.

13. A. J. Durelli, V. J. Parks and S. Uribe, "Optimization of a Slot End Configuration in a Finite Plate Subjected to Uniformly Distributed Load,"--June 1967.
Two-dimensional photoelasticity was used to study various elliptical ends to a slot, and determine which would give the lowest stress concentration for a load normal to the slot length.

14. A. J. Durelli, V. J. Parks and Han-Chow Lee, "Stresses in a Split Cylinder Bonded to a Case and Subjected to Restrained Shrinkage,"--January 1968.
A three-dimensional photoelastic study that describes a method and shows results for the stresses on the free boundaries and at the bonded interface of a solid propellant rocket.

15. A. J. Durelli, "Experimental Stress Analysis Activities in Selected European Laboratories"--August 1968.
This report has been written following a trip conducted by the author through several European countries. A list is given of many of the laboratories doing important experimental stress analysis work and of the people interested in this kind of work. An attempt has been made to abstract the main characteristics of the methods used in some of the countries visited.

16. V. J. Parks, A. J. Durelli and L. Ferrer, "Constant Acceleration Stresses in a Composite Body"--October 1968.
Use of the immersion analogy to determine gravitational stresses in two-dimensional bodies made of materials with different properties.

17. A. J. Durelli, J. A. Clark and A. Kochev, "Experimental Analysis of High Frequency Stress Waves in a Ring"--October 1968.
A method for the complete experimental determination of dynamic stress distributions in a ring is demonstrated. Photoelastic data is supplemented by measurements with a capacitance gage used as a dynamic lateral extensometer.

18. J. A. Clark and A. J. Durelli, "A Modified Method of Holographic Interferometry for Static and Dynamic Photoelasticity"--April 1968.
A simplified absolute retardation approach to photoelastic analysis is described. Dynamic isopachics are presented.

19. J. A. Clark and A. J. Durelli, "Photoelastic Analysis of Flexural Waves in a Bar"--May 1969.
A complete direct, full-field optical determination of dynamic stress distribution is illustrated. The method is applied to the study of flexural waves propagating in a urethane rubber bar. Results are compared with approximate theories of flexural waves.

20. J. A. Clark and A. J. Durelli, "Optical Analysis of Vibrations in Continuous Media"--June 1969.
Optical methods of vibration analysis are described which are independent of assumptions associated with theories of wave propagation. Methods are illustrated with studies of transverse waves in prestressed bars, snap loading of bars and motion of a fluid surrounding a vibrating bar.

21. V. J. Parks, A. J. Durelli, K. Chandrashekhara and T. L. Chen, "Stress Distribution Around a Circular Bar, with Flat and Spherical Ends, Embedded in a Matrix in a Triaxial Stress Field"--July 1969.
A Three-dimensional photoelastic method to determine stresses in composite materials is applied to this basic shape. The analyses of models with different loads are combined to obtain stresses for the triaxial cases.

22. A. J. Durelli, V. J. Parks and L. Ferrer, "Stresses in Solid and Hollow Spheres Subjected to Gravity or to Normal Surface Tractions"--October 1969.
The method described in Report No. 10 above is applied to two specific problems. An approach is suggested to extend the solutions to a class of surface traction problems.

23. J. A. Clark and A. J. Durelli, "Separation of Additive and Subtractive Moiré Patterns"--December 1969.
A spatial filtering technique for adding and subtracting images of several gratings is described and employed to determine the whole field of Cartesian shears and rigid rotations.

24. R. J. Sanford and A. J. Durelli, "Interpretation of Fringes in Stress-Holo-Interferometry"--July 1970.
Errors associated with interpreting stress-holo-interferometry patterns as the superposition of isopachics (with half order fringe shifts) and isochromatics are analyzed theoretically and illustrated with computer generated holographic interference patterns.

25. J. A. Clark, A. J. Durelli and P. A. Laura, "On the Effect of Initial Stress on the Propagation of Flexural Waves in Elastic Rectangular Bars"--December 1970.
Experimental analysis of the propagation of flexural waves in prismatic, elastic bars with and without prestressing. The effects of prestressing by axial tension, axial compression and pure bending are illustrated.

26. A. J. Durelli and J. A. Clark, "Experimental Analysis of Stresses in a Buoy-Cable System Using a Birefringent Fluid"--February 1971.
An extension of the method of photoviscous analysis is presented which permits quantitative studies of strains associated with steady state vibrations of immersed structures. The method is applied in an investigation of one form of behavior of buoy-cable systems loaded by the action of surface waves.

27. A. J. Durelli and T. L. Chen, "Displacements and Finite-Strain Fields in a Sphere Subjected to Large Deformations"--February 1972.
Displacements and strains (ranging from 0.001 to 0.50) are determined in a polyurethane sphere subjected to several levels of diametral compression. A 500 lines-per-inch grating was embedded in a meridian plane of the sphere and moiré effect produced with a non-deformed master. The maximum applied vertical displacement reduced the diameter of the sphere by 27 per cent.

28. A. J. Durelli and S. Machida, "Stresses and Strain in a Disk with Variable Modulus of Elasticity"--March 1972.
A transparent material with variable modulus of elasticity has been manufactured that exhibits good photoelastic properties and can also be strain analyzed by moiré. The results obtained suggests that the stress distribution in the homogeneous disk. It also indicates that the strain fields in both cases are very different, but that it is possible, approximately, to obtain the stress field from the strain field using the value of E at every point, and Hooke's law.

29. A. J. Durelli and J. Buitrago, "State of Stress and Strain in A Rectangular Belt Pulled Over a Cylindrical Pulley"--June 1972.
Two- and three-dimensional photoelasticity as well as electrical strain gages, dial gages and micrometers are used to determine the stress distribution in a belt-pulley system. Contact and tangential stress for various contact angles and friction coefficients are given.

30. T. L. Chen and A. J. Durelli, "Stress Field in a Sphere Subjected to Large Deformations"--June 1972.
Strain fields obtained in a sphere subjected to large diametral compressions from a previous paper were converted into stress fields using two approaches. First, the concept of strain-energy function for an isotropic elastic body was used. Then the stress field was determined with the Hookean type natural stress-natural strain relation. The results so obtained were also compared.

31. A. J. Durelli, V. J. Parks and H. M. Hasseem, "Helices Under Load"--July 1973.
Previous solutions for the case of close coiled helical springs and for helices made of thin bars are extended. The complete solution is presented in graphs for the use of designers. The theoretical development is correlated with experiments.

32. T. L. Chen and A. J. Durelli, "Displacements and Finite Strain Fields in a Hollow Sphere Subjected to Large Elastic Deformations"--September 1973.
The same methods described in No. 27, were applied to a hollow sphere with an inner diameter one half the outer diameter. The hollow sphere was loaded up to a strain of 30 per cent on the meridian plane and a reduction of the diameter by 20 per cent.

33. A. J. Durelli, H. H. Hasseem and V. J. Parks, "New Experimental Method in Three-Dimensional Elastostatics"--December 1973.
A new material is reported which is unique among three-dimensional stress-freezing materials, in that, in its heated (or rubbery) state it has a Poisson's ratio which is appreciably lower than 0.5. For a loaded model, made of this material, the unique property allows the direct determination of stresses from strain measurements taken at interior points in the model.

34. J. Wolak and V. J. Parks, "Evaluation of Large Strains in Industrial Applications"--April 1974.
It was shown that Mohr's circle permits the transformation of strain from one axis of reference to another, irrespective of the magnitude of the strain, and leads to the evaluation of the principal strain components from the measurement of direct strain in three directions.

35. A. J. Durelli, "Experimental Stress Analysis Activities in Selected European Laboratories"--April 1975.
Continuation of Report No. 15 after a visit to Belgium, Holland, Germany, France, Turkey, England and Scotland.

36. A. J. Durelli, V. J. Parks and J. O. Bühler-Vidal, "Linear and Non-linear Elastic and Plastic Strains in a Plate with a Big Hole Loaded Axially in its Plane"--July 1975.
Strain analysis of the ligament of a plate with a big hole indicates that both geometric and material non-linearity may take place. The strain concentration factor was found to vary from 1 to 2 depending on the level of deformation.

37. A. J. Durelli, V. Pavlin, J. O. Bühler-Vidal and G. Ome, "Elastostatics of a Cubic Box Subjected to Concentrated Loads"--August 1975.
Analysis of experimental strain, stress and deflection of a cubic box subjected to concentrated loads applied at the center of two opposite faces. The ratio between the inside span and the wall thickness was varied between approximately 5 and 121.

38. A. J. Durelli, V. J. Parks and J. O. Bühler-Vidal, "Elastostatics of Cubic Boxes Subjected to Pressure"--March 1976.
Experimental analysis of strain, stress and deflections in a cubic box subjected to either internal or external pressure. Inside span-to-wall thickness ratio varied from 5 to 14.

39. Y. Y. Hung, J. D. Hovanesian and A. J. Durelli, "New Optical Method to Determine Vibration-Induced Strains with Variable Sensitivity After Recording"--November 1976.
A steady state vibrating object is illuminated with coherent light and its image slightly misfocused. The resulting specklegram is "time-integrated" as when Fourier filtered gives derivatives of the vibrational amplitude.

40. Y. Y. Hung, C. Y. Liang, J. D. Hovanesian and A. J. Durelli, "Cyclic Stress Studies by Time-Averaged Photoelasticity"--November 1976.
"Time-averaged isochromatics" are formed when the photographic film is exposed for more than one period. Fringes represent amplitudes of the oscillating stress according to the zeroth order Bessel function.

41. Y. Y. Hung, C. Y. Liang, J. D. Hovanesian and A. J. Durelli, "Time-Averaged Shadow Moiré Method for Studying Vibrations"--November 1976.
Time-averaged shadow moiré permits the determination of the amplitude distribution of the deflection of a steady vibrating plate.

ON THE INTERPRETATION OF SHADOW-MOIRÉ FRINGES

by

J. Buitrago and A. J. Durelli

Introduction

The solution of the problem of determining topographical contours of an arbitrary surface can be approached using optical methods. Different techniques can be used depending on the actual depth of the surface, its size and desired sensitivity. Newton rings have a sensitivity of the order on one tenth of the wave length used, but only for a very small range of depth. Holographic interferometry is useful when the depths to record are also very small, is subjected to strict requirements of stability of the instrumentation and is usually expensive.

The simplest method seems to be the projection-grating moiré whereby one projects a grating onto the surface of a plate before deformation and then again after deformation[1][2][3]. The superposition of the deformed and undeformed grating images, when the projection is a parallel one, yields moiré fringes of equal deflection (isothetics w). The method can be applied to surfaces which are originally curved and may then give the isotathmics or loci of equal depth (or height) with respect to a plane of reference. Projection moiré is suitable for relatively large deflections (0.1 mm and up).

Shadow-moiré fringes are produced when the master placed in front of the model interferes with its shadow on the surface of the model. Only one grating is required instead of the two used with the projection grating

method and the surface of the model should be matte in order to receive the shadow of the projected grating.

Shadow-moiré, like the projection-grating method, does not require coherent light and is also of simple implementation. The shadow-moiré patterns may also be isothetics w, (for the case of bent plates for instance) or isostathmics when the observed surface is not originally plane, the fringe pattern giving then the map of the height of points of the surface with respect to the reference plane.

Weller and Shepard[4] were the first to suggest the use of shadow-moiré to determine loci of depth on surfaces. Later Theocaris[5] used the method to measure deflections of flexed plates. Theocaris[6] also generated isopachics by shadow-moiré that in combination with isochromatics were used to separate principal stresses. Successful applications of shadow-moiré techniques to the determination of living bodies topography have been reported by Takasaki[7,8]. Recently, Chiang[9] proposed the uses of a composite grating with two different pitches and Marasco[10] obtained displacements in a hyperboloid-parabolic shell with a non-plane grating.

Interpretation of Shadow-Moiré Fringes

Shadow-moiré fringes can be mathematically interpreted by using communication theory[11,12] although geometric optics suffices to completely analyze the phenomenon.

A geometric approach to the interpretation of shadow-moiré fringes has been published by Pirodda[13]. However, the author did

not consider the effect of rotations of the grating. In what follows a completely general analysis of the shadow-moiré fringes is given including consideration of positions of the grating that require rotations and translation from the normal position defined as the position at which the grating is in contact with the body and is normal to axis of the camera. The influence of these motions on the sensitivity of the system is also considered.

General Equation: Defining the 3-D space by a Cartesian system of coordinates x, y and z, consider any plane x-y where a grating of pitch p has been translated from the model a distance c and then rotated an angle θ, (Fig. 1). The fringe order at an arbitrary point P(x) can be expressed as:

$$n = \frac{(w+c+x\tan\theta_1)}{p}\left\{\frac{(d_z+d_1)\tan\alpha-x}{d_z+d_1+w+c}\cos\theta_1 + \frac{x}{d_z+w+c}\cos\theta_1+\sin\theta_1\left[\frac{(d_z+d_1)\tan\alpha-x}{d_z+d_1+w+c}\tan\left(\theta_1-\tan^{-1}\frac{x}{d_z+w+c}\right)\right.\right.$$
$$\left.\left.+\frac{x}{d_z+w+c}\tan\left(\tan^{-1}\frac{(d_z+d_1)\tan\alpha-x}{d_z+d_1+w+c}+\theta_1\right)\right]\right\} \qquad (1)$$

If the grating is further rotated in the plane y-z (Fig. 2) by an angle θ_2 and in the plane z-x by an angle θ_3 (Fig. 3) Eq. (1) can be made to represent the most general expression for the fringe order at a point when $p/\cos\theta_3$ is substituted for p and $d-(h-z)\sin\theta_2$ for d_z where h is the total height of the model. Equation (1) can also be written in terms of the total distance from the grating to the model by letting $w_t = w + c + x\tan\theta_1$. A detailed derivation of Eq. (1) is presented in the Appendix.

An explicit solution of Eq. (1) for either w or w_t does not seem easy to obtain. However, it is possible to solve it numerically by

redefining it in terms of functions of w or w_t and combining them into the form $F_1(w,n) = F_2(w)$ that can be solved by a trial and error algorithm.

Influence of Rotations and Translation on the Sensitivity: In practical cases it is convenient to position the camera and light source sufficiently far from the model so that d_z is very large compared to $(w + c)$ and to x and consequently $\gamma \approx \alpha$ and $\phi \approx 0$. Under these conditions it is possible to explicitly show the influence of the rotations as well as the translation of the grating plane on the sensitivity of the response of the system. The sensitivity can be quantified as the ratio of the fringe order at a point to its actual distance to the grating (Fig. 1).

a) Rotation about the z axis: Letting $\theta_2 = \theta_3 = 0$ Eq. (1) reduces to

$$n = \frac{1}{p}(w + c + x \tan \theta_1)(\tan\alpha \cos\theta_1 + \sin\theta_1 \tan\alpha \tan\theta_1)$$

therefore the sensitivity

$$s_z = n/w_t = \frac{1}{p} \tan \alpha \sec \theta_1 \qquad (2)$$

By examining Eq. (2), it is seen that for a given depth and pitch the sensitivity varies as the secant of the rotation θ_1. From 0 to 20 degrees, the sensitivity increases only 6% but reaches 41% for θ_1 equal to 45°. However, large values of θ_1 bring the grating plane further apart from the model producing the fading of the fringes. The increase in sensitivity has to be compromised with the quality of the fringes.

b) Rotation about x axis: Letting $\theta_1 = \theta_2 = 0$, Eq. (1) becomes

$$n/w_t = \frac{1}{p} \frac{(d_z+d_1)\tan \alpha - x}{d_z+d_1+w+c} = \frac{1}{p} \tan \alpha \tag{3}$$

Since $\tan \alpha = f/(d_z + d_1)$ and $d_z = d-(h-z)\sin \theta_2$ the sensitivity is given by

$$s_x = \frac{1}{p} \frac{f}{d-(h-z) \sin \theta_2} \tag{4}$$

If $d \gg (h-z)$ the change in sensitivity obtained by rotating the grating plane about the x axis is neglible.

c) Rotation about y axis: Letting $\theta_1 = \theta_2 = 0$ in Eq. (1) gives

$$s_y = \frac{1}{p} \cos \theta_3 \tan \alpha \tag{5}$$

In this instance the sensitivity is proportional to the cosine of the angle of rotation. As θ_3 approaches 90° the pitch becomes very large ($p' = p/\cos \theta_3$) and the fringes fade. The sensitivity decreases as θ_3 increases.

d) Rigid translation in the x-y plane: In this case $\theta_1 = \theta_2 = \theta_3 = 0$ and the sensitivity is expressed by

$$s_t = \frac{1}{p} \tan \alpha \tag{6}$$

Translation of the grating plane does not bring about any change in the sensitivity but as in case a) will tend to produce weaker fringes. Translation of the grating plane is of no practical interest.

Simplified Equations: Three cases of practical importance, determined by the number of elements used in the system will be considered. The

grating will touch the body and its plane will be perpendicular to the axis of the camera.

a) Point source and camera: In Eq. (1) let $\theta_1 = \theta_2 = \theta_3 = c=0$ (Fig. 4) The distance d_z becomes constant and the fringe order at representative points 1 and 2 is given by

$$n_{1,2} = \frac{w}{p} \left[\frac{(d+d_1)\tan\alpha - x}{d + d_1 + w} + \frac{x}{d + w} \right] \tag{7}$$

It can be noted from Eq. (7) that if the body has a plane of symmetry coinciding with the y - z plane, the fringe pattern will not be symmetric because of the sign of x. In practice the zero fringe order is arbitrarily assigned to the point of contact between the grating and the surfaces. Knowing the fringe order, the grating pitch and the geometry of the optical system, Eq. (7) can be solved for w as follows

$$w = -\frac{1}{2} k \pm \sqrt{\frac{1}{4} k^2 + \frac{npd}{tg\alpha}} \tag{8}$$

where

$$k = \frac{d[(d+d_1)\ tg\alpha - x - np] - np(d+d_1) + x(d+d_1)}{(d+d_1)\ tg\alpha - np}$$

The + or - sign in Eq. (8) is selected to obtain the desired sign for w. Eq. (8) is valid for any z.

A case of practical importance occurs when the source and the camera focusing plane lay on a plane that is parallel to the grating plane. Letting $d_1 = 0$ in Eq. (7) the fringe order is given by

$$n_{1,2} = \frac{w}{p} \left[\frac{dtg\alpha - x}{d+w} + \frac{x}{d+w} \right] = \frac{dtg\alpha}{d+w} \ \frac{w}{p} \tag{9}$$

It can be observed from this expression that the fringe pattern will be symmetric with respect to x if the body is symmetric with respect to z. Substituting now tanα by f/d, the displacement w is given by

$$w = \frac{npd}{f-np} \tag{10}$$

b) Collimated incident light and camera: If in the previous set-up a collimator is added between the source and the grating Fig. (5) the object receives incident parallel rays of light. This is equivalent to locating the source at an infinite distance from the object. Taking the limit of Eq. (7), as d_1 approaches infinity, the fringe order is given by

$$n_{1,2} = \frac{w}{p}\left[tg\alpha + \frac{x}{d+w}\right] \tag{11}$$

Again the pattern corresponding to a symmetric body will not be symmetric because of the sign of x. Solving for w in Eq. (11)

$$w = -\frac{1}{2}k_1 - \sqrt{\frac{1}{4}k_1^2 + \frac{npd}{tg\alpha}} \tag{12}$$

where

$$k_1 = \frac{d - np + x}{tg\alpha}$$

c) Collimated incident and reflected light: This condition can be obtained by inserting another collimator, this one between the grating and the camera as depicted in Fig. (6). In this instance the fringe order can be arrived at by letting $d_1 + d$ go to infinity in Eq. (7). Then

$$n_{1,2} = \frac{w}{p} - tg\alpha$$

thus (13)

$$w = \frac{np}{tg\alpha}$$

Experimental Considerations

Set up: Of the simplified cases presented above, the last one seems to be the most attractive because of the simplicity of Eq. (13). Unfortunately, as the bodies grow larger, wider collimated beams are required, which in

turn implies larger diameter lenses. When of good quality, these lenses are difficult to obtain at a reasonable cost.

The use of a point source of light and a camera appears to have practical advantages although the analysis of the pattern is more complicated (Eq. 8). However, a simplified expression can be obtained when the source and camera are on a plane parallel to the grating (Eq. 10). This three element system (source, grating and camera) is frequently the most advantageous.

Sensitivity: The sensitivity of the method is a direct function of the pitch of the grating and the angle of observation. Very small pitches cannot be used because the very fine gratings diffract the light. The The appropriate pitch and angle of observation have to be selected for the particular range of heights to be measured.

Fringe Definition: When coarse gratings are used, it is advantageous to have a thin light source parallel to the direction of the grating lines to minimize the penumbra. The thinner the source the sharper the fringes. It should be remembered that shadow-moiré fringes are formed at planes located at different distances from the grating plane and should be photographed using small diaphram apertures. When the bodies to be studied have a plane of symmetry, it is advisable to use two light sources symmetrically located with respect to the camera axis to avoid that the fringes that appear on the side near one source of light present different intensity than the fringes at the opposite side.

Fringe definition may also be lost at areas at which the gradients are steep. In these cases it is recommended to move the grating during the exposure[6,11].

Sources: White light sources of about 500 to 1000 watts are usually required to generate proper intensity. Incandescent filament lamps are most commonly used and the filament is then aligned with the grating lines. To sharpen the fringes illumination can be passed through a slit, but this decreases the intensity.

Application

To experimentally verify some of the previously developed equations, a sphere 6.9 in (175 mm) in diameter was analyzed. For convenience, the selected set-up consisted of a point light source and a camera laying on a plane parallel to the grating. The fringe pattern shown in Fig. 7 is symmetric as predicted by Eq. (9) for symmetric surfaces. Surface depths referred to the grating plane (tangent to the sphere) were computed using Eq. (10) and compared to the values obtained from geometry. Fig. 8 shows this comparison. The agreement is very good.

As a more general application of the shadow-moiré technique, the anticlastic surface of a perforated tube, turned inside out was also studied (Fig. 9). The optical arrangement consisted of collimated incident light and camera. In this instance, even though the surface is symmetric with respect to x, the fringe order is not (Fig. 10) in accordance with Eq. (11), where the alternate sign of x for two points symmetrically located about the vertical axis yields different values of n. To further illustrate this effect, the fringe order n has been represented along three different lines on the surface of the tube. On the vertical axis, where $x = 0$, the fringe distribution exhibits complete symmetry. However, for any other off-the-vertical-axis line asymmetry appears, reaching a maximum along the horizontal axis. The actual depths, on the other hand, have to remain symmetric and can be obtained using Eq. (12).

Acknowledgments

The research program reported in this paper is part of a dissertation prepared by J. Buitrago as requirement for a Ph.D. degree to be awarded at Catholic University in Washington, D.C. The program has been supported financially in part with funds of the John F. Dodge Chair at Oakland University, in Rochester, Michigan and funds from Office of Naval Research Contract N00014-76-C-0487 with N. Perrone as monitor.

REFERENCES

1. Hovanesian J. D., Haskell R. E. and Powell R. L., "Use of a Projected Ruling Moiré Method for Vibration and Deflection Measurement of Three-Dimensional Structures," Proc. Eng. Applications of Holography (Symposium), Los Angeles, Feb. 16-18, 1972.
2. Chiang F. P. and Khetan R. P., "A Moiré Method for Measuring Large Deflection of Shells," State Univ. of NY at Stony Brook, College of Eng. Report No. 221, Feb. 1972. Paper presented at SESA Spring Meeting, 1972. (Research in Progress.)
3. Khetan R. P., "Theory and Applications of Projection Moiré Methods," Ph.D. Dissertation, Dept. of Mechanics, State Univ. of NY at Stony Brook, May 1975.
4. Weller R. and Shepard M., "Displacement Measurements by Mechanical Interferometry," Proc. Soc. Exp. Str. Anal., Vol VI, No. 1, 1948.
5. Theocaris P.S., Proc. Int. Symp. Shell Struct., Warsaw 1963, North Holland Publ. Co., Amsterdam, PP. 887, 1965.
6. Theocaris P. S., "Isopachic Patterns by Moiré Method," J. Exp. Mech., Vol. 4, No. 6, June 1964.
7. Takasaki H., "Moiré Topography," App. Opt. Vol. 9, No. 6, pp. 1467-1472, June 1970
8. Takasaki H., "Moiré Topography," App. Opt. Vol. 12, No. 2, pp. 845-850, Apr. 1973.
9. Chiang F. P., "A Shadow Moiré Method with Two Discrete Sensitivities," Exp. Mech., Vol. 15, No. 10, pp. 382-385, Oct. 1975.

10. Marasco J., "Use of a Curved Grating in Shadow Moiré," Exp. Mech., Vol. 15, No. 12, Dec. 1975.

11. Meadows D. M. and Johnson W. D., "Generation of Surface Contours by Moiré Patterns," App. Opt., Vol. 9, No. 4, pp. 942-947, April 1970.

12. Allen J. B. and Meadows D. M., "Removal of Unwanted Patterns from Moiré Contours Maps by Grid Translation Techniques," App. Opt., Vol. 10, No. 1, pp. 210-212, Jan. 1971.

13. Pirodda L., "Principie Applicazioni di un Metodo Fotogrametrico Basado sull' Impiego Moiré," Rivista di Ingegneria, No. 12, Dec. 1969.

14. Durelli A. J and Parks V. J., Moiré Analysis of Strain, Mac-Graw Hill, p. 66, 1970.

APPENDIX: General Equation for Interpretation of Shadow-Moiré

Referring to Fig. 1, consider the grating plane that has been translated along the y axis an amount c from the highest point on an arbitrary surface S and subsequently rotated through an angle θ_1, about the z axis (positive rotation according to the vectorial product convention). The fringe order corresponding to the interference of the shadow cast at the point P and the grating itself is simply,

$$n = a'/p \tag{A.1}$$

a' being the distance measured on the grating plane between the incident and reflected rays, and p the pitch of the grating. Since only one grating is used, dark areas of the grating interfere with their own shadows and consequently the integer fringe orders correspond to light fringes while the half orders to dark fringes[14] (Fig. 7)

From geometry it is seen that

$$a' = [(a_1+a_2)\cos\theta_1 + e + g)]/p \tag{A.2}$$

where

$$a_1+a_2 = (w+c+x\ \tan\theta_1)(\tan\gamma + \tan\phi) \tag{A.3}$$

$$e = a_2\ \sin\theta_1\tan(\theta_1-\phi) = (w+c+x\ \tan\theta_1)\tan\gamma\ \sin\theta_1\tan(\theta_1-\phi) \tag{A.4}$$

and

$$g = a_1\ \sin\theta_1\tan(\theta_1+\gamma) = (w+c+x\ \tan\theta_1)\tan\phi\sin\theta_1\tan(\theta_1+\gamma) \tag{A.5}$$

γ and ϕ are the angles the incident and the reflected rays make with the normal to the contacting normal position of the grating plane respectively and w the depth of the point P from that position.

Equations (A.3), (A.4) and (A.5) are now substituted into Eq. (A.2). After collecting terms a' is

$$a' = (w+c+x\ \tan\theta_1)\{(\tan\gamma+\tan\phi)\cos\theta_1+\sin\theta_1[\tan\gamma\tan(\theta_1-\phi)+\tan\phi\tan(\gamma+\theta_1)]\} \tag{A.6}$$

$$\tan\gamma = \frac{f-x}{d_z+d_1+w+c} \tag{A.7}$$

and

$$\tan\phi = \frac{x}{d_z+w+c} \tag{A.8}$$

where d_z is the variable distance between the camera and the grating plane for the different x = constant planes as produced by the rotation of the grating about the x axis. According to Fig. 2, d_z can be expressed as

$$d_z = d - (h-z)\sin\theta_2 \tag{A.9}$$

h representing the total height of the model and d the constant distant between the camera and the original position of the grating. Moreover, the distance f between the camera optical axis and the point light source is

$$f = (d_z + d_1)\tan\alpha \tag{A.10}$$

α is referred to as the illumination angle and d_1 is the distance between the camera and the source measured along the axis of the camera.

Using the expressions for d_z and f in (A.7) and (A.8), the tangents of γ and ϕ are then given by

$$\tan\gamma = \frac{[d-(h-z)\sin\theta_2+d_1]\tan\alpha}{d-(h-z)\sin\theta_2+d_1+w+c} \tag{A.11}$$

$$\tan\phi = \frac{x}{d-(h-z)\sin\theta_2+w+c} \tag{A.12}$$

Now, eliminating the $\tan\gamma$ and $\tan\phi$ from (A.6) using (A.11) and (A.12), and dividing through by the pitch modified by the grating rotation θ_3 (Fig. 3) about y, the fringe order as determined by Eq. (A.1) finally is obtained as

$$n = \frac{(w+c+x\tan\theta_1)}{p\cos\theta_3}\{[\frac{<d-(h-z)\sin\theta_2+d_1>\tan\alpha - x}{d-(h-z)\sin\theta_2+d_1+w+c} + \frac{x}{d-(h-z)\sin\theta_2+w+c}]\cos\theta_1$$

$$+ \sin\theta_1[\frac{<d-(h-z)\sin\theta_2+d_1>\tan\alpha-x}{d-(h-z)\sin\theta_2+d_1+w+c}\tan(\theta_1-\tan^{-1}\frac{x}{d-(h-z)\sin\theta_2+w+c})$$

$$+ \frac{x}{d-(h-z)\sin\theta_2+w+c}\tan(\tan^{-1}\frac{<d-(h-z)\sin\theta_2+d_1>\tan\alpha - x}{d-(h-z)\sin\theta_2+d_1+w+c}+\theta_1)]\} \tag{A.13}$$

It can be concluded, therefore, that the most general interpretation of the shadow moiré fringe order at any point on an arbitrary surface can completely be defined in terms of the geometry of the optical system lay-out and the rotations and translation of the grating plane. Translations perpendicular to the camera axis do not affect the fringe value.

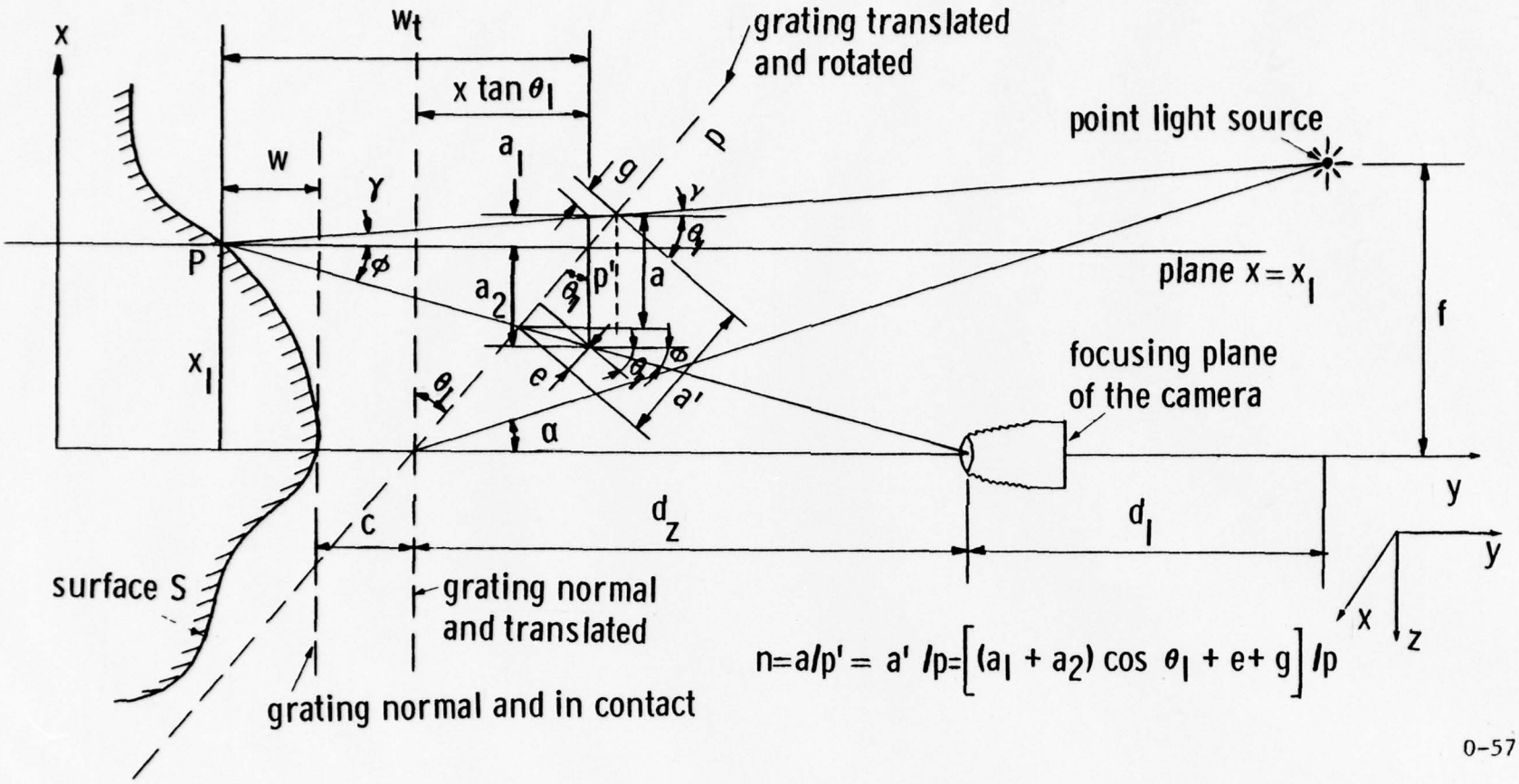

Fig. 1 Shadow Moire Fringe Interpretation on an Arbitrary Surface Using a Point Source and Camera When the Grating Has Been Rotated and Translated in the x-y Plane

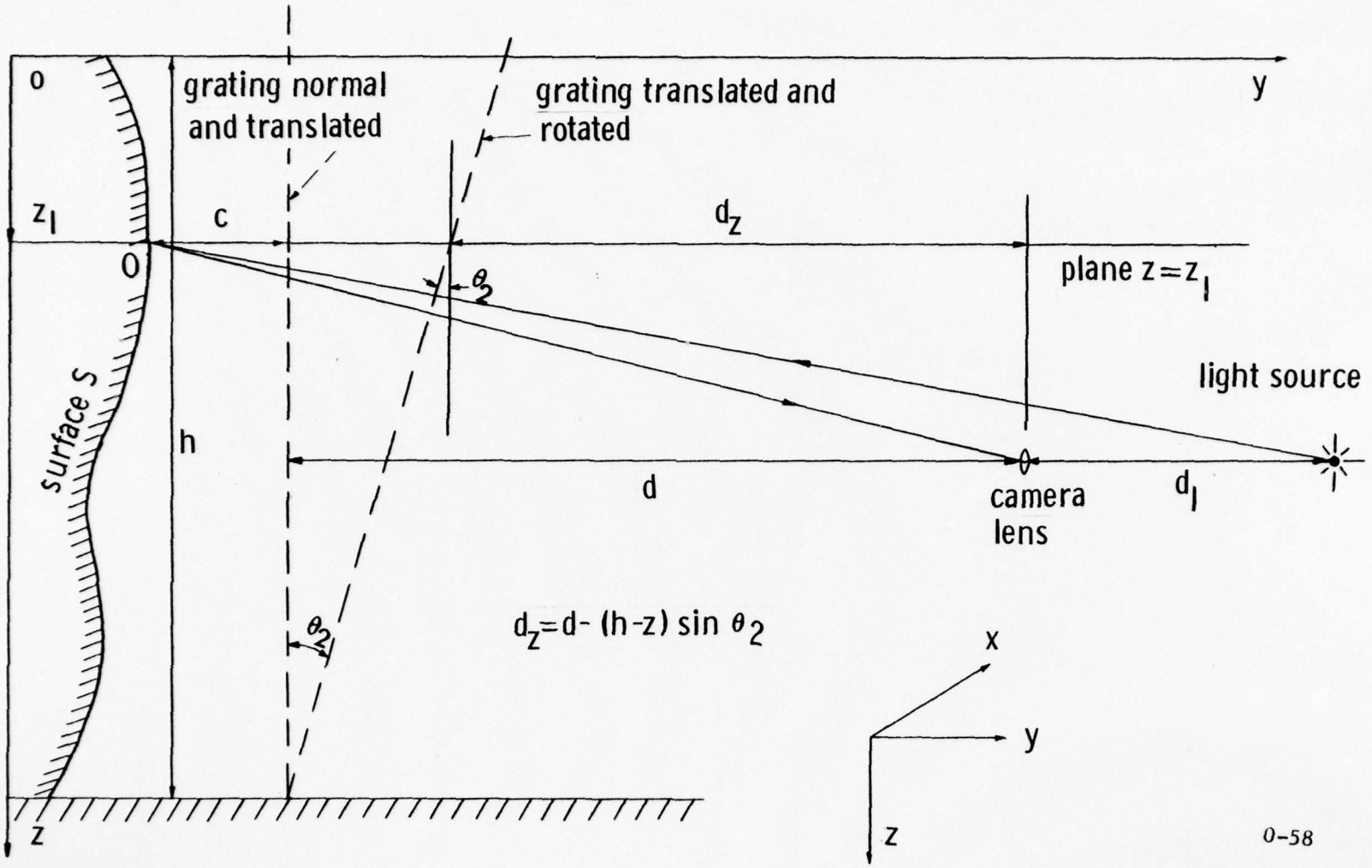

Fig. 2 Effect of the Rotation of theGrating in the y-z Plane on the Interpretation of the Shadow Moire Fringes Obtained Using a Point Source and Camera, on an Arbitrary Surface

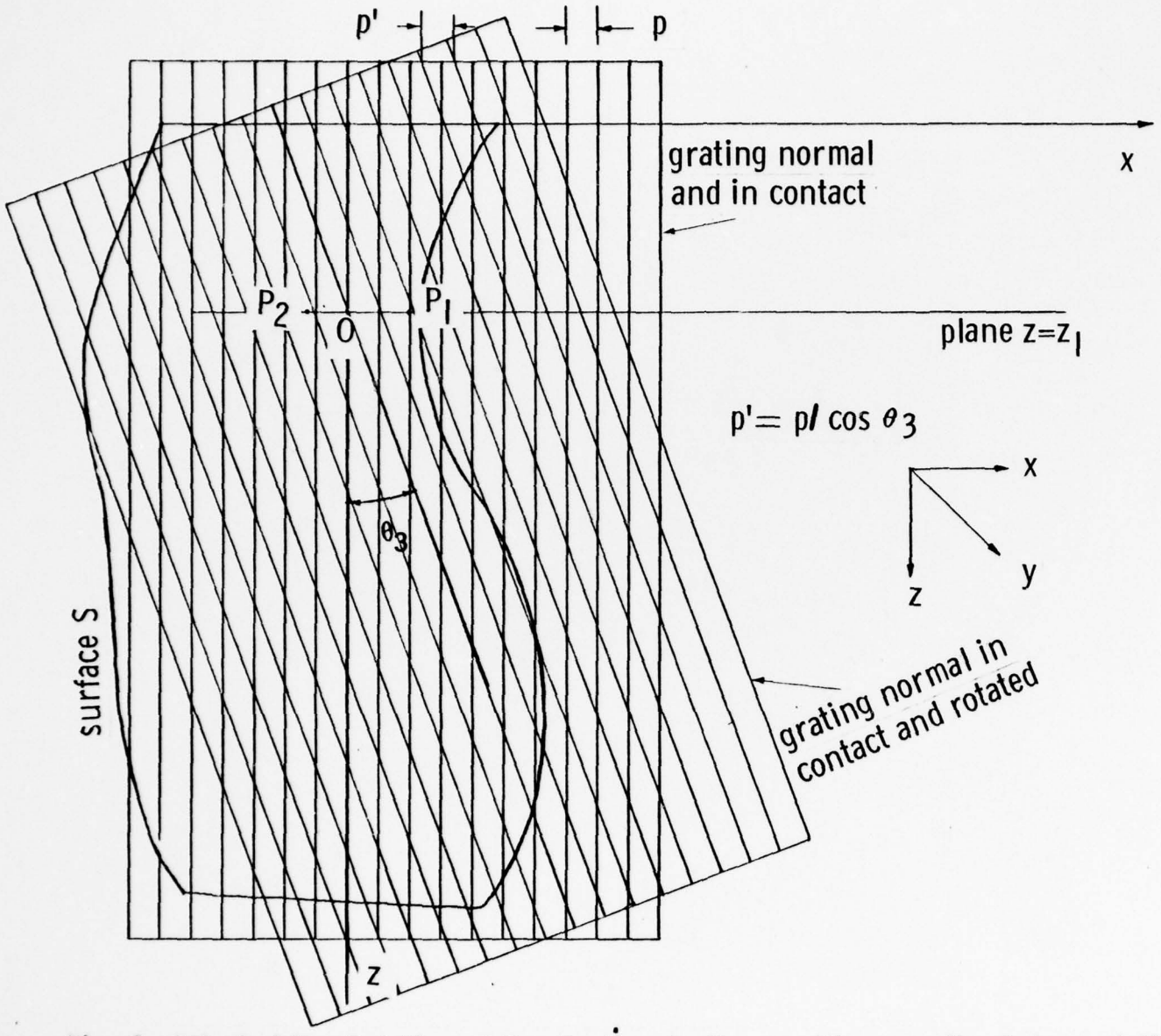

0-59

Fig. 3 Effect of the Rotation of the Grating in the z-x Plane on the Interpretation of the Shadow Moire Fringes Obtained Using a Point Source and Camera, on an Arbitrary Surface

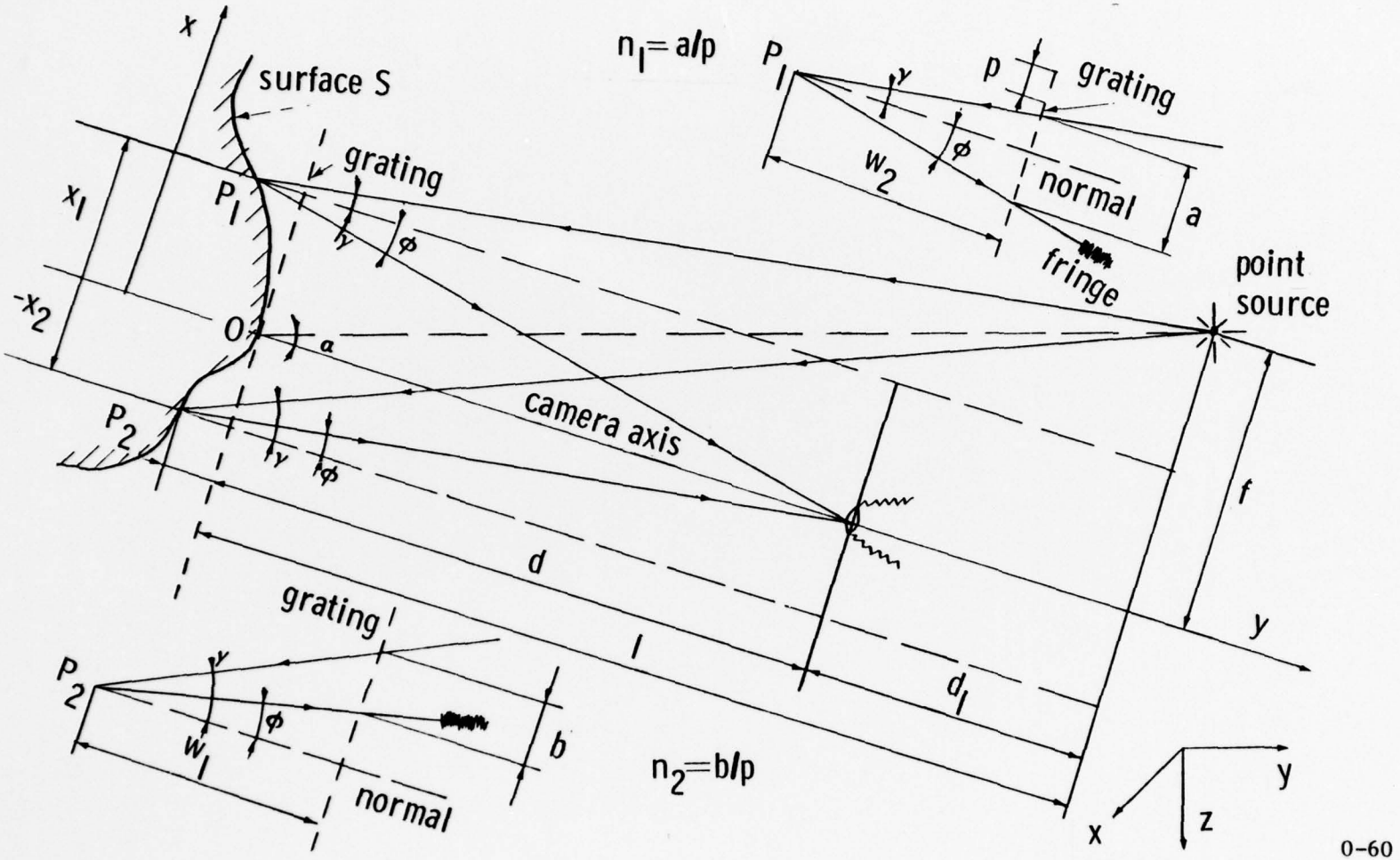

Fig. 4 Interpretation of the Shadow Moire Fringes Obtained Using A Point Source and Camera, on an Arbitrary Surface

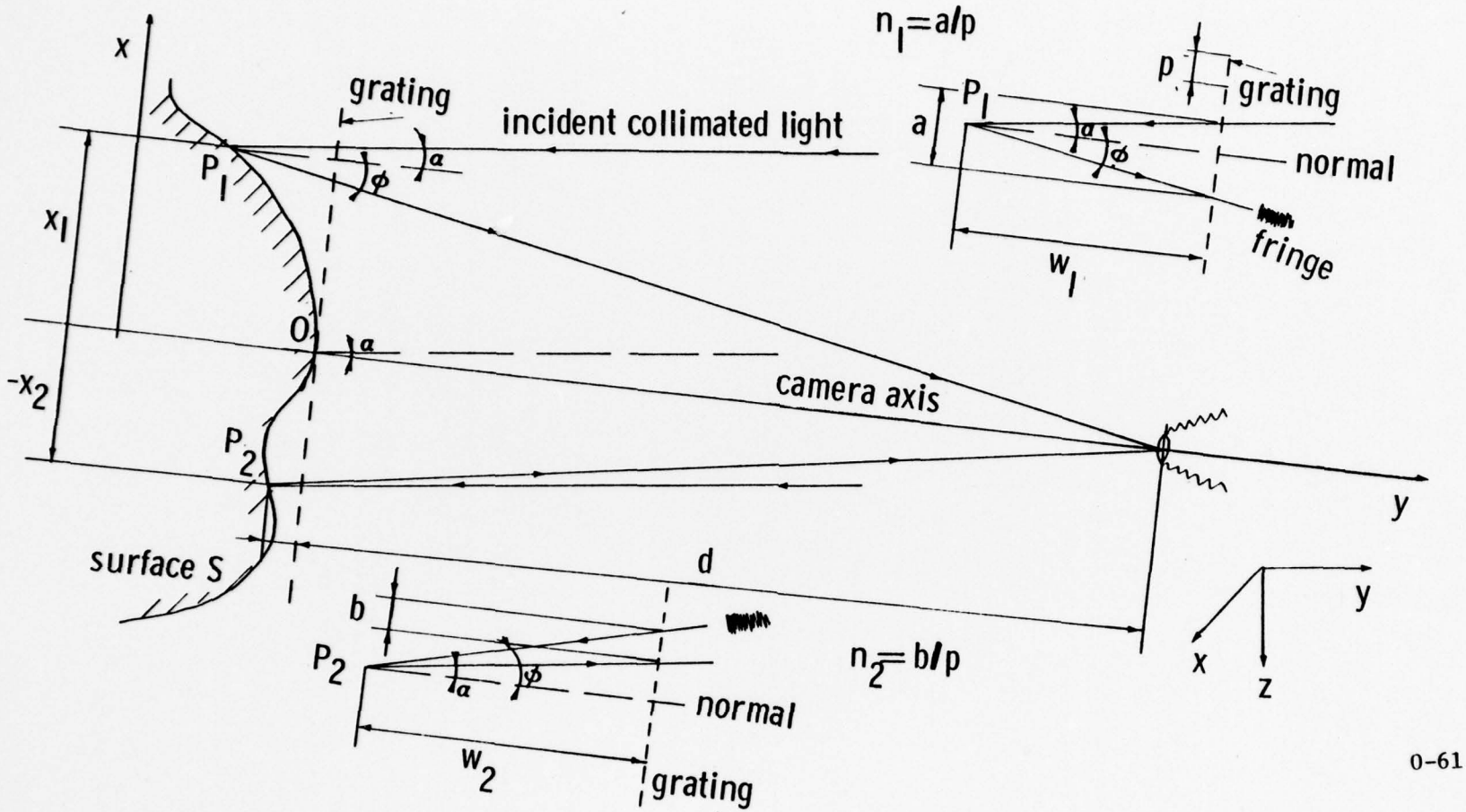

Fig. 5 Interpretation of the Shadow Moire Fringes Obtained Using Incident Collimated Light and Camera, on an Arbitrary Surface

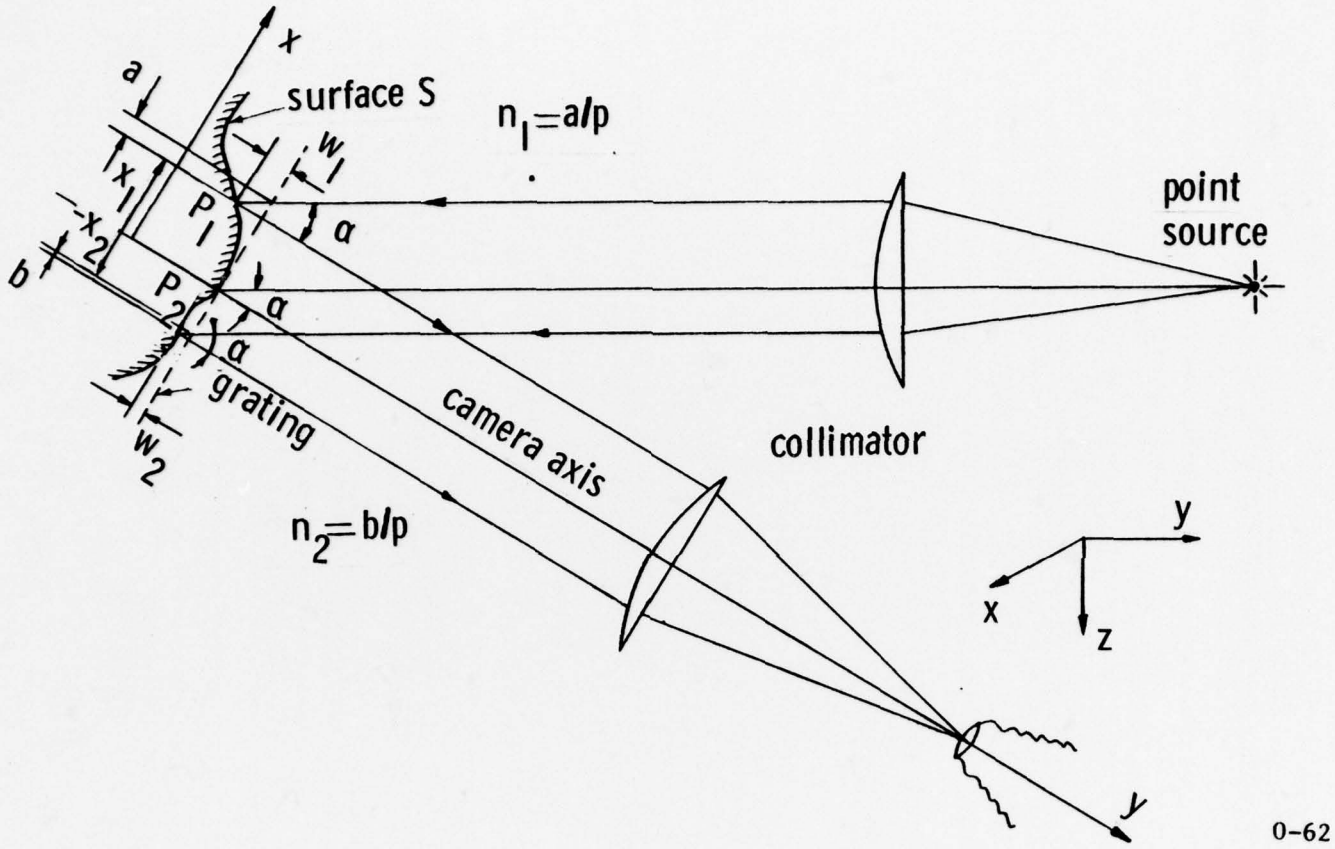

Fig. 6 Interpretation of the Shadow Moire fringes Obtained Using Collimated Incident and Reflected Light, on an Arbitrary Surface

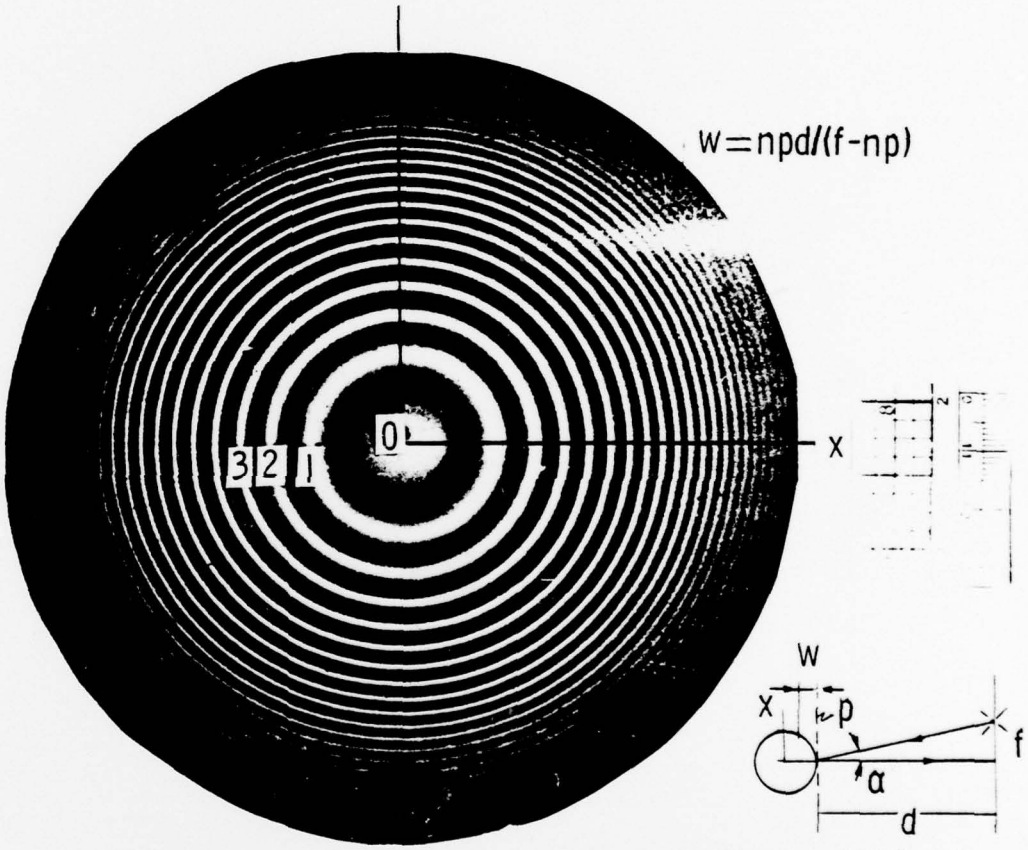

Fig. 7 Isostathmics of a Spherical Surface Obtained Using Shadow-Moire. Camera and Light Source on a Plane Parallel to the Grating

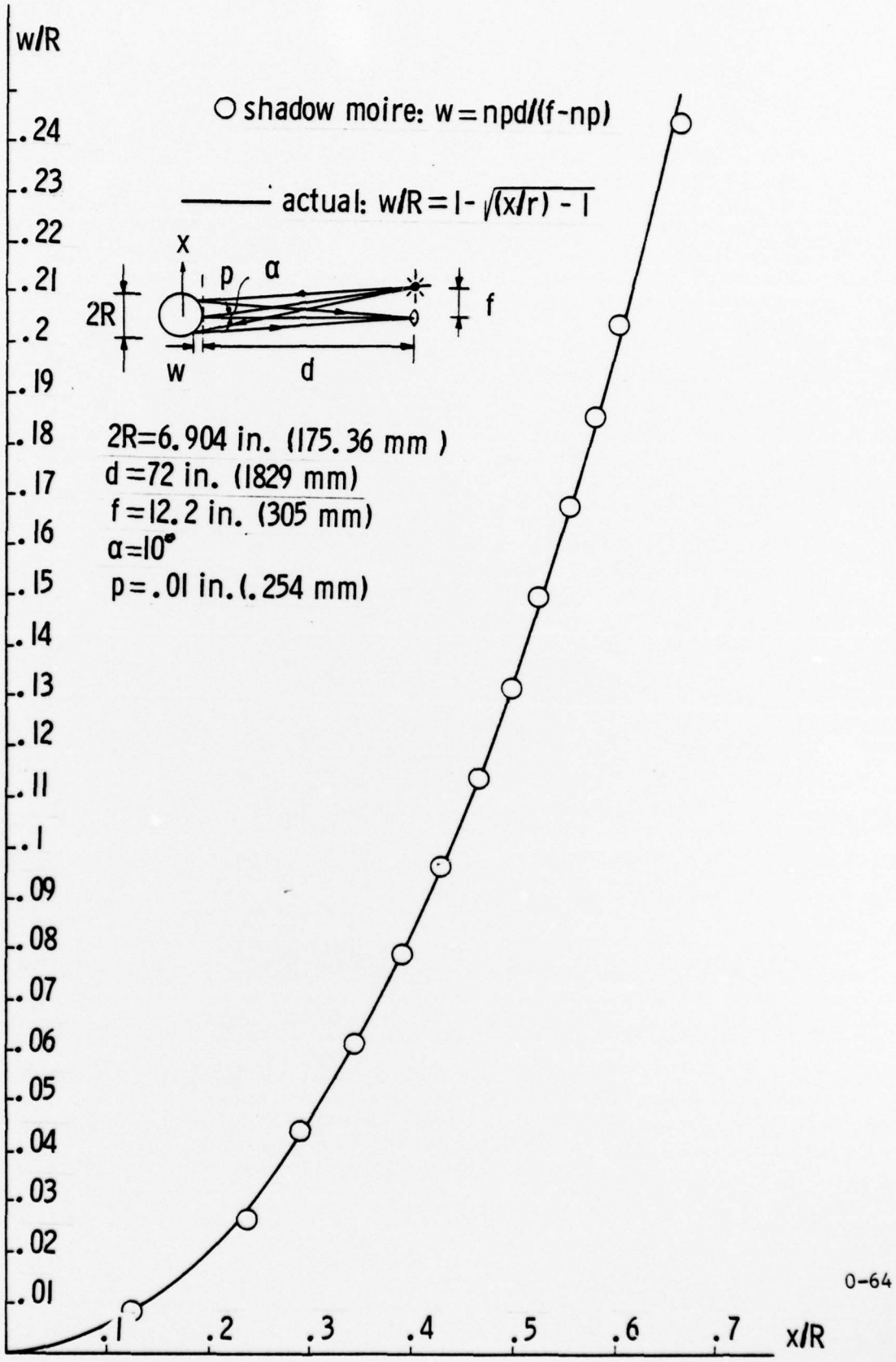

Fig. 8 Depth of a Spherical Surface from the Grating Plane Tangent to the Surface, Obtained Using Shadow Moire Fringes Produced Having the Camera and Light Source on a Plane Parallel to the Grating

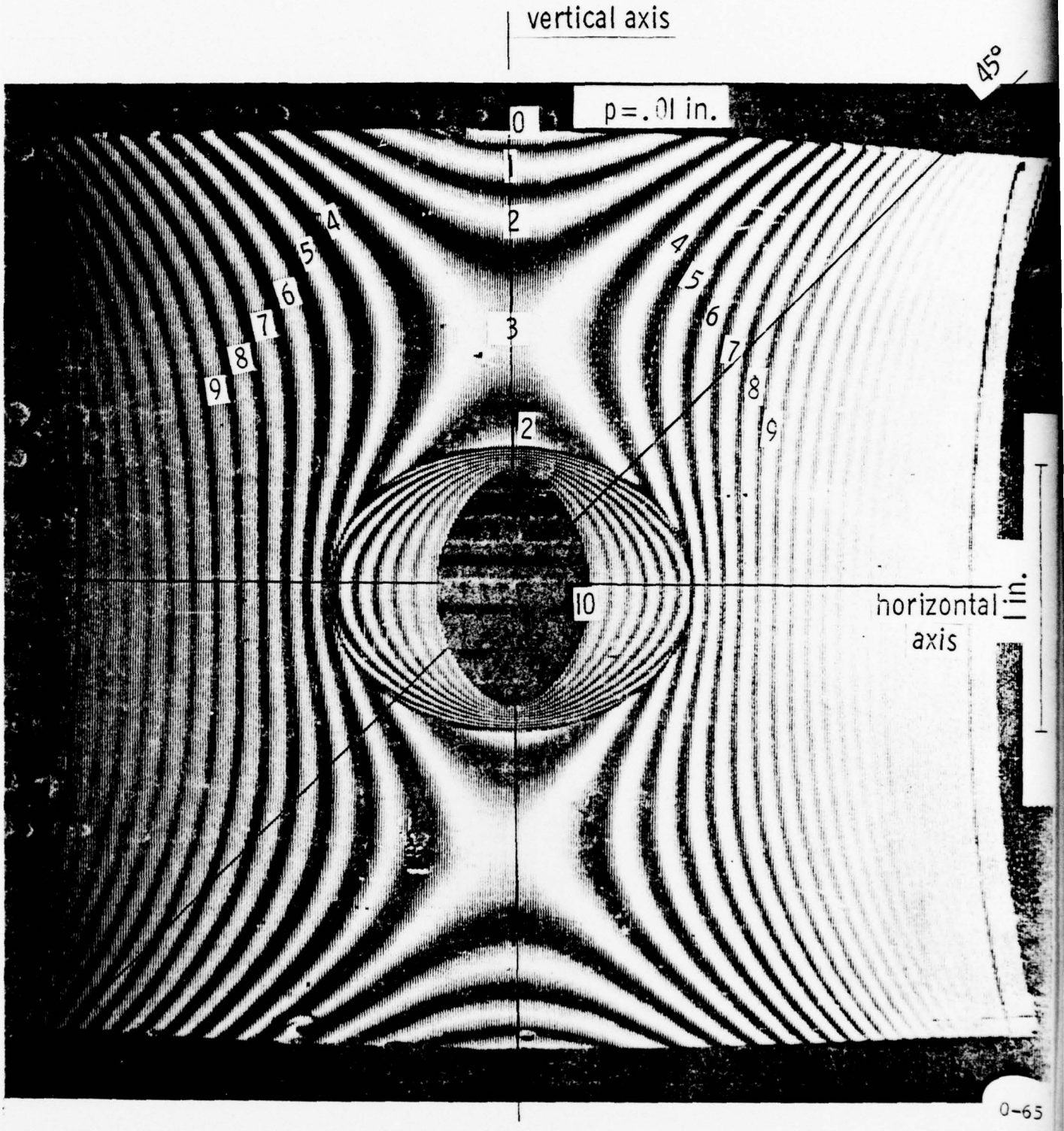

Fig. 9 Loci of Points of Equal Depth on the Outer Surface of a Multi-Perforated Inverted Tube Obtained Using Shadow-Moire. Parallel Incident Light and Camera $n=(w/p)(\tan\alpha + x/(d+w))$

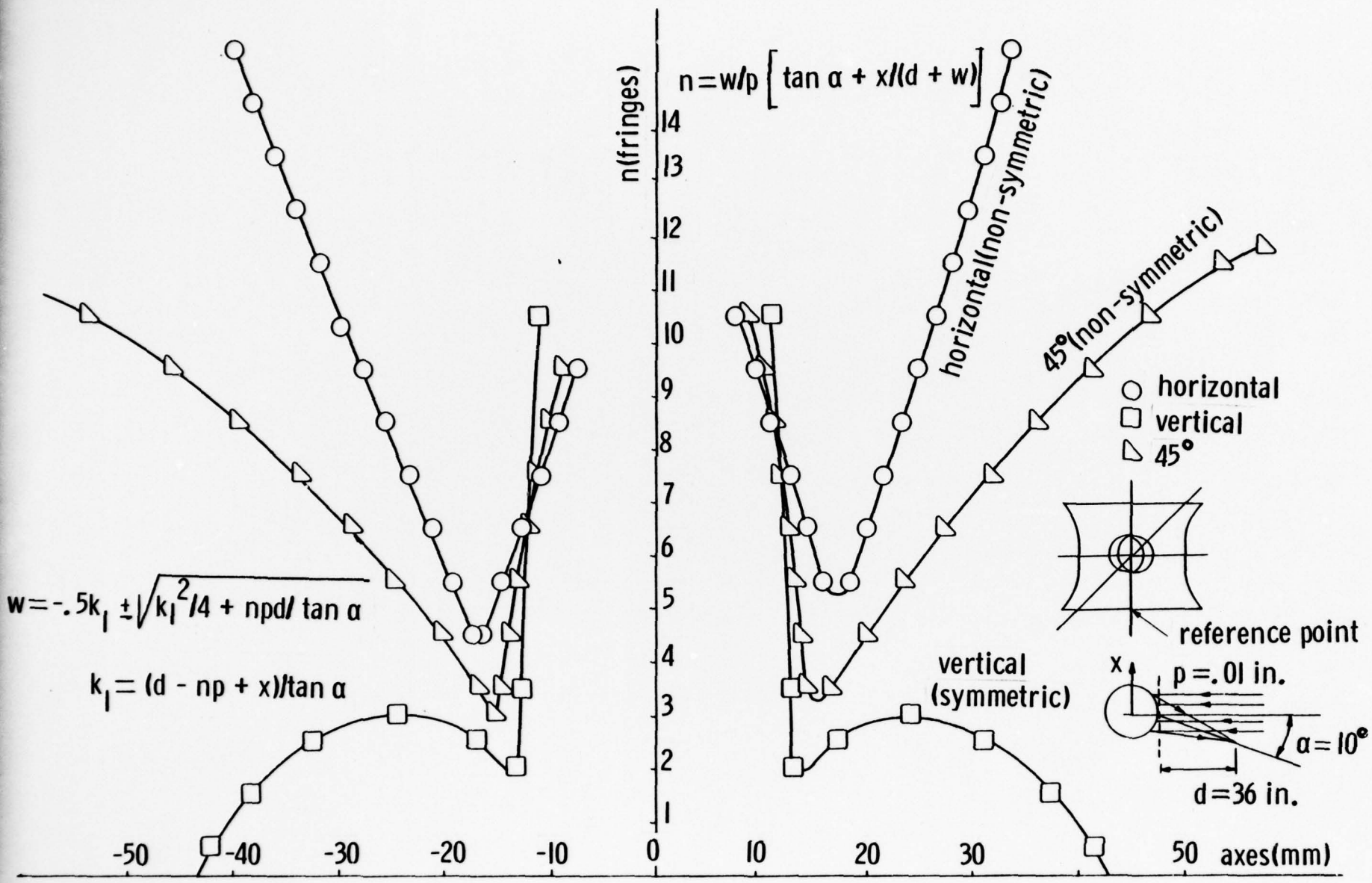

Fig. 10 Shadow Moire Fringe Order on Vertical, Horizontal, and at 45 ^{0} Lines on the Outer Surface of a Multi-Perforated Inverted Tube

0-66

ONR DISTRIBUTION LIST

Part I - Government

Chief of Naval Research
Department of the Navy
Arlingon, Virginia 22217
Attn: Code 474 (2)
471
222

Director
ONR Branch Office
495 Summer Street
Boston, Massachusetts 02210

Director
ONR Branch Office
536 S. Clark Street
Chicago, Illinois 60604

Director
Naval Research Laboratory
Attn: Code 2629 (ONRL)
Washington, D.C. 20390 (6)

U.S. Naval Research Laboratory
Attn: Code 2627
Washington, D.C. 20390

Commanding Officer
ONR Branch Office
207 West 24th Street
New York, N.Y. 10011

Director
ONR Branch Office
1030 E. Green Street
Pasadena, California 91101

Defense Documentation Center
Cameron Station
Alexandria, Virginia 22314 (12)

Army

Commanding Officer
U.S. Army Research Off. Durham
Attn: Mr. J. J. Murray
CRD-AA-IP
Box CM, Duke Station
Durham, North Carolina 27706

Commanding Officer
AMXMR-ATL
Attn: Mr. R. Shea
U.S. Army Materials Res. Agency
Watertown, Massachusetts 02172

Watervliet Arsenal
MAGGS Research Center
Watervliet, New York 12189
Attn: Director of Research

Redstone Scientific Info. Center
Chief, Document Section
U.S. Army Missile Command
Redstone Arsenal, Alabama 35809

Army R &D Center
Fort Belvoir, Virginia 22060

Navy

Commanding Officer & Director
Naval Ship Res. & Dev. Center
Bethesda, Maryland 20034
Attn: Code 042 (Tech. Lib. Br.)
17 (Struc. Mech. Lab.)
172
172
174
177
1800(Appl. Math. Lab.)
5412S (Dr. W.D. Sette)
19 (Dr. M.M. Sevik)
1901 (Dr. M. Strassberg)
1945
196 (Dr. D. Feit)
1962

Naval Weapons Laboratory
Dahlgren, Virginia 22448

Naval Research Laboratory
Washington, D.C. 203
Attn: Code 8400
8410
8430
8440
6300
6390
6380

Undersea Explosion Res. Div.
Naval Ship R&D Center
Norfolk Naval Shipyard
Portsmouth, Virginia 23709
Attn: Dr. E. Palmer
Code 780

Naval Ship Res. & Dev. Center
Annapolis Division
Annapolis, Maryland 21402
Attn: Code 2740 - Dr. Y. F. Wang
28 - Mr. R.J. Wolfe
281 - Mr. Niederberger
2814 - Dr. H. Vanderveldt

Technical Library
Naval Underwater Weapons Center
Pasadena Annex
3202 E. Foothill Blvd.
Pasadena, California 91107

U.S. Naval Weapons Center
China Lake, California 93557
Attn: Code 4062 - Mr. W. Werback
4520 - Mr. Ken Bischel

Commanding Officer
U.S. Naval Civil Engr. Lab.
Code L31
Port Hueneme, California 93041

Technical Director
U.S. Naval Ordnance Lab.
White Oak
Silver Spring, Maryland 20910

Technical Director
Naval Undersea R&D Center
San Diego, California 92132

Supervisor of Shipbuilding
U.S. Navy
Newport News, Virginia 23607

Techanical Director
Mare Island Naval Shipyard
Vallejo, California 94592

U.S. Navy Underwater Sound Ref. Lab.
Office of Naval Research
P.O. Box 8337
Orlando, Florida 32806

Chief of Naval Operations
Dept. of the Navy
Washington, D.C. 20350
Attn: Code Op07T

Strategic Systems Project Off.
Department of the Navy
Washington, D.C. 20390
Attn: NSP- 001 Chief Scientist

Deep Submergence Systems
Naval Ship Systems Command
Code 39522
Department of the Navy
Washington, D.C. 203 60

Engineering Dept.
U.S. Naval Academy
Annapolis, Maryland 21402

Naval Air Systems Command
Dept. of the Navy
Washington, D.C. 20360
Attn: NAVAIR 5302 Aero & Struc.
5308 Struc.
52031F Materials
604 Tech. Lib.

Director, Aero Mechanics
Naval Air Development Center
Johnsville
Warminster, Pennsylvania 18974

Technical Director
U.S. naval Undersea R&D Center
San Diego, California 92132

Engineering Department
U.S. Naval Academy
Annapolis, Maryland 21402

Naval Facilities Engineering Command
Dept. of the Navy
Washington, D.C. 20360
Attn: NAVFAC 03 Res. & Dev.
04 Res. & Dev.
14114 Tech. Lib.

Naval Sea Systems Command
Dept. of the Navy
Washington, D.C. 20360
Attn: NAVSHIP 03 Res. & Tech.
031 Ch.Scientist R&D
03412 Hydromechanics
037 Ship Silencing Div.
035 Weapons Dynamics

Navy cont.

Naval Ship Engineering Center
Prince George's Plaza
Hyattsville, Maryland 20782
Attn: NAVSEC 6100 Ship Sys Engr & Des Dep
6102C Computer-Aided Ship Des
6105G
6110 Ship Concept Des
6120 Hull Div.
6120D Hull Div.
6128 Surface Ship Struct.
6129 Submarine Struct.

Air Force

Commander WADD
Wright-Patterson Air Force Base
Dayton, Ohio 45433
Attn: Code WWRMDD
AFFDL (FDDS)
Structures Division
AFLC (MCEEA)

Chief, Applied Mechanics Group
U.S. Air Force Inst. of Tech.
Wright-Patterson Air Force Base
Dayton, Ohio 45433

Chief, Civil Engineering Branch
WLRC, Research Division
Air Force Weapons Laboratory
Kirtland AFB, New Mexico 87117

Air Force Office of Scientific Research
1400 Wilson Blvd.
Arlington, Virginia 22209
Attn: Mechanics Div.

NASA

Structures Research Division
National Aeronautics & Space Admin.
Langley Research Center
Langley Station
Hampton, Virginia 23365

National Aeronautic & Space Admin.
Associate Administrator for Advanced Research & Technology
Washington, D.C. 02546

Scientific & Tech. Info. Facility
NASA Representative (S-AK/DL)
P.O. Box 5700
Bethesda, Maryland 20014

Other Government Activities

Commandant
Chief, Testing & Development Div.
U.S. Coast Guard
1300 E. Street, N.W.
Washington, D.C. 20226

Technical Director
Marine Corps Dev & Educ. Command
Quantico, Virginia 22134

Director
National Bureau of Standards
Washington, D.C. 20234
Attn: Mr. B.L. Wilson, EN 219

Dr. M. Gaus
National Science Foundation
Engineering Division
Washington, D.C. 20550

Science & Tech. Division
Library of Congress
Washington, D.C. 20540

Director
Defense Nuclear Agency
Washington, D.C. 20305
Attn: SPSS

Commander Field Command
Defense Nuclear Agency
Sandia Base
Albuquerque, New Mexico 87115

Director Defense Research & Engr
Technical Library
Room 3C-128
The Pentagon
Washington, D.C. 20301

Chief, Airframe & Equipment Branch
FS-120
Office of Flight Standards
Federal Aviation Agency
Washington, D.C. 20553

Chief, Research and Development
Maritime Administration
Washington, D.C. 20235

Deputy Chief, Office of Ship Constr.
Maritime Administration
Washington, D.C. 20235
Attn: Mr. U.L. Russo

Atomic Energy Commission
Div. of Reactor Devel. & Tech.
Germantown, Maryland 20767

Ship Hull Research Committee
National Research Council
National Academy of Sciences
2101 Constitution Avenue
Washington, D.C. 20418
Attn: Mr. A.R. Lytle

Part 2 - Contractors and Other Technical Collaborators

Universities

Dr. J. Tinsley Oden
University of Texas at Austin
345 Eng. Science Bldg.
Austin, Texas 78712

Prof. Julius Miklowitz
California Institute of Technology
Div. of Engineering & Applied Sci.
Pasadena, California 91109

Dr. Harold Liebowitz, Dean
School of Engr. & Applied Science
George Washington University
725 - 23rd St., N.W.
Washington, D.C. 20006

Prof. Eli Sternberg
California Institute of Technology
Div. of Engr. & Applied Sciences
Pasadena, California 91109

Prof. Paul M. Naghdi
University of California
Div. of Applied Mechanics
Etcheverry Hall
Berkeley, California 94720

Professor P.S. Symonds
Brown University
Division of Engineering
Providence, R.I. 02912

Prof. A.J. Durelli
John F. Dodge Professor
Oakland University
Rochester, Michigan 48063

Prof. R.B. Testa
Columbia University
Dept. of Civil Engineering
S.W. Mudd Bldg.
New York, New York 10027

Prof. H.H. Bleich
Columbia University
Dept. of Civil Engineering
Amsterdam & 120th St.
New York, New York 10027

Prof. F.L. DiMaggio
Columbia University
Dept. of Civil Engineering
616 Mudd Building
New York, New York 10027

Prof. A.M. Freudenthal
George Washington University
School of Engineering & Applied Science
Washington, D.C. 20006

D.C. Evans
University of Utah
Computer Science Division
Salt Lake City, Utah 84112

Prof. Norman Jones
Massachusetts Inst. of Technology
Dept. of Naval Architecture & Marine Engrng
Cambridge, Massachusetts 02139

Asst. to Secretary Defense
Atomic Energy-Att. D. Cotter
Washington, D.C. 20301

Dr. V.R. Hodgson
Wayne State University
School of Medicine
Detroit, Michigan 48202

Universities cont.

Dean B.A. Boley
Northwestern University
Technological Institute
2145 Sheridan Road
Evanston, Illinois 60201

Prof. P.G. Hodge, Jr.
University of Minnesota
Dept. of Aerospace Engng & Mech.
Minneapolis, Minnesota 55455

Dr. D.C. Drucker
University of Illinois
Dean of Engineering
Urbana, Illinois 61801

Prof. N.M. Newmark
University of Illinois
Dept. of Civil Engineering
Urbana, Illinois 61801

Prof. E. Reissner
University of California, San Diego
Dept. of Applied Mechanics
La Jolla, California 92037

Prof. William A. Nash
University of Massachusetts
Dept. of Mechanics & Aerospace Eng.
Amherst, Massachusetts 01002

Library (Code 0384)
U.S. Naval Postgraduate School
Monterey, California 93940

Prof. Arnold Allentuch
Newark College of Engineering
Dept. of Mechanical Engineering
323 High Street
Newark, New Jersey 07102

Dr. George Herrmann
Stanford University
Dept. of Applied Mechanics
Stanford, California 94305

Prof. J.D. Achenbach
Northwestern University
Dept. of Civil Engineering
Evanston, Illinois 60201

Director, Applied Research Lab.
Pennsylvania State University
P.O. Box 30
State College, Pennsylvania 16801

Prof. Eugen J. Skudrzyk
Pennsylvania State University
Applied Research Laboratory
Dept. of Physics - P.O. Box 30
State College, Pennsylvania 16801

Prof. J. Kempner
Polytechnic Institute of Brooklyn
Dept. of Aero. Engrg & Applied Mech.
333 Jay Street
Brooklyn, N.Y. 11201

Prof. J. Klosner
Polytechnic Institute of Brooklyn
Dept. of Aerospace & Appl. Mech.
333 Jay Street
Brooklyn, N.Y. 11201

Prof. R.A. Schapery
Texas A&M University
Dept. of Civil Engineering
College Station, Texas 77840

Prof. W.D. Pilkey
University of Virginia
Dept. of Aerospace Engineering
Charlottesville, Virginia 22903

Dr. H.G. Schaeffer
University of Maryland
Aerospace Engineering Dept.
College Park, Maryland 20742

Prof. K.D. Willmert
Clarkson College of Technology
Dept. of Mechanical Engineering
Potsdam, N.Y. 13676

Dr. J.A. Stricklin
Texas A&M University
Aerospace Engineering Dept.
College Station, Texas 77843

Dr. L.A. Schmit
University of California, LA
School of Engineering & Applied Sci.
Los Angeles, California 90024

Dr. H.A. Kamel
The University of Arizona
Aerospace & Mech. Engineering Dept.
Tucson, Arizona 85721

Dr. B.S. Berger
University of Maryland
Dept. of Mechanical Engineering
College Park, Maryland 20742

Prof. G.R. Irwin
Dept. of Mechanical Engng.
University of Maryland
College Park, Maryland 20742

Dr. S.J. Fenves
Carnegie-Mellon University
Dept. of Civil Engineering
Schenley Park
Pittsburgh, Pennsylvania 15213

Dr. Ronald L. Huston
Dept. of Engineering Analysis
Mail Box 112
University of Cincinnati
Cincinnati, Ohio 45221

Prof. George Sih
Dept. of Mechanics
Lehigh University
Bethlehem, Pennsylvania 18015

Prof. A.S. Kobayashi
University of Washington
Dept. of Mechanical Engineering
Seattle, Washington 98105

Librarian
Webb Institute of Naval Architecture
Crescent Beach Road, Glen Cove
Long Island, New York 11542

Prof. Daniel Frederick
Virginia Polytechnic Institute
Dept. of Engineering Mechanics
Blacksburg, Virginia 24061

Prof. A.C. Eringen
Dept. of Aerospace & Mech. Sciences
Princeton University
Princeton, New Jersey 08540

Dr. S.L. Koh
School of Aero., Astro. & Eng. Sc.
Purdue University
Lafayette, Indiana 47907

Prof. E.H. Lee
Div. of Engrg. Mechanics
Stanford University
Stanford, California 94305

Prof. R.D. Mindlin
Dept. of Civil Engrg
Columbia University
S.W. Mudd Building
New York, N.Y. 10027

Prof. S.B. Dong
University of California
Dept. of Mechanics
Los Angeles, California 90024

Prof. Burt Paul
University of Pennsylvania
Towne School of Civil & Mech Engr
Rm. 113 - Towne Building
220 S. 33rd Street
Philadelphia, Pennsylvania 19104

Prof. J.W. Liu
Dept. of Chemical Engr. & Metal.
Syracuse University
Syracuse, N.Y. 13210

Prof. S. Bodner
Technion R&D Foundation
Haifa, Israel

Prof. R.J.H. Bollard
Chairman, Aeronautical Engr. Dept.
207 Guggenheim Hall
University of Washington
Seattle, Washington 98105

Prof. G.S. Heller
Division of Engineering
Brown University
Providence, Rhode Island 02912

Prof. Werner Goldsmith
Dept. of Mechanical Engineering
Div. of Applied Mechanics
University of California
Berkeley, California 94720

Prof. J.R. Rice
Division of Engineering
Brown University
Providence, R.I. 02912

Prof. R.S. Rivlin
Center for the Application of
Mathematics
Lehigh University
Bethlehem, Pennsylvania 18015

Bell Telephone Labs Inc.
505 King Avenue -Tech. Lib.
Columbus, OH 43201

Dr. Francis Cozzarelli
Div. of Interdisciplinary
Studies & Research
School of Engineering
State University of New York
Buffalo, N.Y. 14214

Industry and Research Institutes

Library Services Dept.
Report Section Bldg. 14-14
Argonne National Laboratory
9700 S. Cass Avenue
Argonne, Illinois 60440

Dr. M.C. Junger
Cambridge Acoustical Associates
129 Mount Auburn St.
Cambridge, Massachusetts 02138

Dr. L.H. Chen
General Dynamics Corporation
Electric Boat Division
Groton, Connecticut 06340

Dr. J.E. Greenspon
J.G. Engineering Research Assoc.
3831 Menlo Drive
Baltimore, Maryland 21215

Dr. S. Batdorf
The Aerospace Corp.
P.O. Box 92957
Los Angeles, California 90009

Dr. K.C. Park
Lockheed Palo Alto Research Lab.
Dept. 5233, Bldg. 205
3251 Hanover St.
Palo Alto, CA 94304

Library
Newport News Shipbuilding & Dry
Dock Company
Newport News, Virginia 23607

Dr. W.F. Bozich
McDonnell Douglas Corporation
5301 Bolsa Avenue
Huntington Beach, CA 92647

Dr. H.N. Abramson
Southwest Research Institute
Technical Vice President
Mechanical Sciences
P.O. Drawer 28510
San Antonio, Texas 78284

Dr. R.C. DeHart
Southwest Research Institute
Dept. of Structural Research
P.O. Drawer 28510
San Antonio, Texas 78284

Dr. M.L. Baron
Weidlinger Associates, Consulting
Engineers
110 East 59th Street
New York, N.Y. 10022

Dr. W.A. Von Riesmann
Sandia Laboratories
Sandia Base
Albuquerque, New Mexico 87115

Dr. T.L. Geers
Lockheed Missiles & Space Co.
Palo Alto Research Laboratory
3251 Hanover Street
Palo Alto, California 94304

Dr. J.L. Tocher
Boeing Computer Services, Inc.
P.O. Box 24346
Seattle, Washington 98124

Mr. William Caywood
Code BBE, Applied Physics Laboratory
8621 Georgia Avenue
Silver Spring, Maryland 20034

Mr. P.C. Durup
Lockheed-California Company
Aeromechanics Dept., 74-43
Burbank, California 91503

Assistant Chief for Technology
Office of Naval Research, Code 200
Arlington, Virginia 22217

Los Alamos Scientific Lab
P.O. Box 1663 - Tech Libs
Los Alamos, NM 87544

Boeing Company
Attn. Aerospace Lab
P.O. Box 3707
Seattle, WA 98124

IIT Research Institute
10 West 35th Street
Chicago, ILL 60616

Unclassified

SECURITY CLASSIFICATION OF THIS PAGE (When Data Entered)

REPORT DOCUMENTATION PAGE

READ INSTRUCTIONS BEFORE COMPLETING FORM

1. REPORT NUMBER: 42

2. GOVT ACCESSION NO.:

3. RECIPIENT'S CATALOG NUMBER:

4. TITLE (and Subtitle): ON THE INTERPRETATION OF SHADOW-MOIRE FRINGES

5. TYPE OF REPORT & PERIOD COVERED: (14) 42

6. PERFORMING ORG. REPORT NUMBER:

7. AUTHOR(s): J. Buitrago, Catholic University, Washington, D.C.
A. J. Durelli, John [redacted] Professor, Oakland University, Rochester, MI

8. CONTRACT OR GRANT NUMBER(s): N00014-76-C-0487 (15)

9. PERFORMING ORGANIZATION NAME AND ADDRESS:
Catholic University
Washington, D.C. 20064

10. PROGRAM ELEMENT, PROJECT, TASK AREA & WORK UNIT NUMBERS: (12) 36 p.

11. CONTROLLING OFFICE NAME AND ADDRESS:
Office of Naval Research
Department of the Navy
Washington, D.C. 20025

12. REPORT DATE: April 1977

13. NUMBER OF PAGES: 36

14. MONITORING AGENCY NAME & ADDRESS (if different from Controlling Office):

15. SECURITY CLASS. (of this report): None

15a. DECLASSIFICATION/DOWNGRADING SCHEDULE:

16. DISTRIBUTION STATEMENT (of this Report)

Distribution of this report is unlimited

17. DISTRIBUTION STATEMENT (of the abstract entered in Block 20, if different from Report)

18. SUPPLEMENTARY NOTES

19. KEY WORDS (Continue on reverse side if necessary and identify by block number)

Moiré
contours
Experimental Stress Analysis
Deflection measurements
Isotathmics
inverted tube

20. ABSTRACT (Continue on reverse side if necessary and identify by block number)

Shadow-moiré is presented as one of several means of determining loci of constant height in curved surfaces (isotathmics). A general expression to interpret the fringes is derived taking into consideration possible rotations and translation of the grating. A discussion of the influence of such rotations and translation on the sensitivity of the response is also presented. Furthermore, simplified equations are obtained for particular cases of practical interest. An example of application to the

DD FORM 1 JAN 73 1473 EDITION OF 1 NOV 65 IS OBSOLETE
S/N 0102-014-6601

405 252

SECURITY CLASSIFICATION OF THIS PAGE (When Data Entered)

case of an inverted perforated tube is shown.